Separation and Purification Technology 276 (2021) 119306

Contents lists available at ScienceDirect

Separation and Purification Technology

journal homepage: www.elsevier.com/locate/seppur

Considering solubility disparity and acoustic-cavitation susceptivity of neoteric solvents to accurately predict sono-recovery yield of value-added compounds

Pengxu Wang [a], Yaqin Ma [a,b,*], Chen Zhang [a], Meng Jia [a]

[a] Citrus Research Institute, Southwest University, Chongqing 400712, People's Republic of China
[b] National Engineering Research Center for Citrus, Chongqing 400712, People's Republic of China

ARTICLE INFO

Keywords:
Ultrasound
Neoteric solvents
Solubility parameters
Sono-recovery
Bubble radius

ABSTRACT

This work aimed to theoretically predict the sono-recovery yield of value-added compounds in various neoteric solvents through considering solubility difference and acoustic-cavitation variability. Preferentially, the solvent-solute compatibility was calculated by Hansen solubility parameters (HSPs), but unexpectedly the results showed that the HSPs prediction was not preferably consistent with the tendency of extraction yield. Subsequently, calculated correlations between maximum bubble radius (MBR) and solvent properties showed the following hierarchies: viscosity (-0.86^{**}) > density (-0.83^{**}) > surface tension (-0.64^{**}), and MBR can be considered as a mirror of solvent properties to reflect the flavonoids yield ($r = 0.75^{**}$) but that was inapplicable to phenolic acids ($r = 0.33$). Evidentially, micromorphological observation exhibited that significant modification of epidermis had an intense disposition to occur in the solvents with greater MBR such as methanol, water and ethyl acetate. No significant sonochemiluminescence (SCL) signal was captured including aqueous malic acid/choline chloride (ChCl), lactic acid/ChCl, sucrose/ChCl, methanol, ethyl lactate, and glycerol, but the addition of ChCl into alcohols can enhance the production of free radicals. The generation of free radicals was independent of MBR and their impacts on final compounds presented pluralist and limited effects. In addition, how to more accurately quantify the effects of free radicals on the final compounds is still a poser. Overall, This work constructed a bridge between theoretical calculation and laboratory data and demonstrated the fundamentality of maximum bubble radius in the biorefinery of value-added compounds.

1. Introduction

The sustainable and renewable economy to promote the evolution of traditionally biological waste treatment or efficient conversion has become an imminent task as emphasized by the United Nations General Assembly in the title of "Transforming Our World: The 2030 Agenda for Sustainable Development" [1]. In this context, a central project to achieve a cradle-to-cradle circular economy is to develop bio-based or sustainable solvents to replace conventionally petroleum-based solvents and maximize biotransformation of agro-industrial residues while decreasing adverse impacts and menace on human beings and our planet. Neoteric solvents tremendously emphasized sustainability, biodegradability, and long-term impacts on the ecosystem [2] and were precisely classified into five kinds including aqueous solvent systems, deep eutectic solvents, ionic liquids, bio-based solvents (e.g. ethanol, ethyl lactate, etc.) and switchable solvent systems (CO_2) [3]. In comparison with traditional solvents, deep eutectic solvents (DESs) have a succession of advantages such as high thermal stability, lower toxicity and excellent solubility [4,5]. Nam and coworkers [6] using tailor-made DESs to recovery flavonoids from *Flos sophorae* found that the extractability improved 3% compared with preeminently methanol-based extraction craft. Besides, it is worth mentioning that several bio-based solvents such as glycerol and ethyl lactate have been commercialized and advanced towards diversity and versatility [7]. Hitherto, the library of neoteric solvent is gigantic and the ranking of solvents and the establishment of screening guides is an essential tactic that is being employed to generate immediate results for ascertaining targeted solvent [8]. But there is no systematic demarche to guide this time-demanding procedure.

Accordingly, regardless of biochemicals recovery or biorefinery, the

* Corresponding author at: Citrus Research Institute, Southwest University, Chongqing 400712, People's Republic of China.
E-mail address: myaya211@cric.cn (Y. Ma).

https://doi.org/10.1016/j.seppur.2021.119306
Received 2 April 2021; Received in revised form 12 July 2021; Accepted 12 July 2021
Available online 18 July 2021

assistance of process intensification technology to reduce energy consumption and improve process efficiency is also a pivotal demarche to achieve sustainable chemical society, for instance, ultrasound-assisted methodology [9,10]. Ultrasound as a mechanical wave is propagated in the elastic medium providing enough energy to overcome the cohesive forces of a liquid and further induces the movement of the liquid molecules giving rise to the generation of cavity thereby growth and collapse of bubbles via a series of compression and rarefaction waves. When these bubbles expand to their critical size and then collapse extremely, which will release shock waves and microjets to attack and destruct the surrounding substances. Employing this intensification technology has been a huge advance such as achieving the diversified extraction of bioactive ingredients (142 phytochemicals) from *Annona crassiflora* Mart. [11] and recovering the phenolic compounds from different fractions of *Eugenia calycina* Cambess (leaves, fruit, pulp, and seed) [12] as well as obtaining better economic benefits to meet sustainable development [13].

Generally, those solvents with low viscosity, low vapor pressure, and low surface tension are conducive to the formation of high-energy cavitation [14,15]. But regrettably, most neoteric solvents exhibit higher viscosity or lower mobility than conventional solvents even adopting an appropriate dilution procedure [16]. If a liquid medium has a high viscosity, which can induce an increment in sound attenuation, and a prolongation in coalescence time of bubbles as well as a decrease in cavitation volume [17] and bubble surface instability [18]. Surface tension has a weak effect on bubble growth but it can limit bubble nucleation and coalescence probability giving rise to a decrease in bubble size and oscillation phase [18]. Meanwhile, high-viscosity liquid can cause a long-period damped oscillation of bubble resulting in a lower collapse strength in the final collapsing phase [19]. In this sense, acoustic-cavitation variability due to multifarious properties of sustainable solvents will become a hindrance and challenge.

Although aforementioned neoteric solvents present remarkable potentials to meet the trend of sustainable chemistry, typical practical conundrum is how wide difference of physicochemical properties in particular viscosity or surface tension limit the process intensification of ultrasound, which has not been addressed [20]. Besides, although acoustic cavitation-based intensification technology provides the robust energy and aggressiveness to enhance the mixing, mass transfer, and releasing compounds, it is not clear the role that the solute-solvent compatibility plays in the ultrasonic intensification process. A trial and error system for the calculation of the compatibility during the pre-intensification stage is to use Hansen solubility parameters (HSPs) that is based on an assumption that the total cohesive energy is divided into three forces encompassing dispersion force (δ_d), dipole force (δ_p) and hydrogen-bonding force (δ_h). Aware of this, Kantar et al. [21] once introduced HSPs and Fick's second law as a decision-making tool to extract naringin from grapefruit peels and elaborated the intensification mechanism of pulsed electric field and practicability of HSPs prediction.

As far as we all know, continuous efforts towards the multi-parameter operation and synergistic application of innovative technology have been widely explored [22]. Nevertheless, integrating multiple physical and chemical properties of sustainable solvent into a single protocol to study the complex nonlinear process of cavitation technology and the compatibility profiles necessitates intensive modeling and experimental validation to further achieve the integration of scheduling, control, and accurate prediction, which has not been addressed. This work aimed to probe the sono-recovery mechanism in wide sustainable solvents (deep eutectic solvents, bio-based solvent, water and polyethylene glycol) to explain the intensification process of value-added compounds (six phenolic acids: ferulic acid, sinapic acid, p-coumaric acid, p-hydroxybenzoic acid, vanillic acid and caffeic acids; five flavonoids: hesperidin, nobiletin, didymin, narirutin and sinensetin) and to weigh the feasibility towards theoretical predication from multidimensional numerical simulation or calculation. This work also supplied the integration among miscellaneous decision-making tools towards the controllability of the intensified process contributing to substantial cost savings and improved performance.

2. Materials and methods

2.1. Dynamic viscosity

The dynamic viscosity of all solvents (Table 1) was measured at room temperature (25 °C) using a viscometer (DV2T, Brookfield Engineering Labs., Inc., USA) equipped with an ultra-low adapter allowing to measure low-viscosity liquid such as water, ethanol and so on. Test volume and temperature were maintained at 20 mL and 25 ± 2 °C, respectively.

2.2. Surface tension

The surface tension of various solvents (Table 1) was measured by a contact angle meter (SDC-200S, Dongguan Dingsheng Precision Instrument Co., Ltd., China). Each sample was measured 100 times continuously with an interval of 1 s, and the average value was calculated at last.

2.3. Speed of sound

The speed of the sound wave (Table 1) in various solvents was calculated according to the speed correlating with surface tension and liquid density [23]. The equation is as follows:

$$u = 10^{\left(0.6199 \cdot \log_{10}\left(\frac{\sigma}{\rho}\right) + 5.94\right)} \quad (1)$$

where u is the speed of sound (m/s), σ is the surface tension (mN/m), ρ is the liquid density (Kg/m^3).

2.4. Instrument and operating parameters

A probe-type equipment equipped with a titanium horn microtip of 15 mm diameter (JY98-IIIN, Ningbo Scientz Biotechnology Co. Ningbo, China) was used. Liquid volume was recommended by the equipment manufacturer (Ningbo Scientz Biotechnology Co) because too large liquid volume was detrimental to keep the constant working temperature but too little liquid volume could lead to the spatter of a liquid. Working temperature (65 °C) was selected based on our former work. Previously, we investigated the parameter dependence of sonochemical and mechanical effects of ultrasound and founded that high temperatures (55–70 °C) can inhibit the production of free radicals to some extent [24]. But the results from our and many other papers showed that temperature above 70 °C can lead to the degradation/deterioration of unstable bio-compounds[25]. Thus, the temperature was slightly adjusted to 65 °C. The sonication time (20 min) was chosen according to the two-site kinetic model. Generally, the extraction yield of 70–90% of polyphenols occurred in the first 5–20 min and tended to achieve the equilibrium after 15 min [26].

2.5. Calculation of compatibility

Hansen solubility parameters (HSPs) of the solvent system and targeted compounds were calculated based on the total cohesive energy (E) that is divided into the dispersion force [δ_d, (MJ/cm^3)$^{1/2}$], dipole force [δ_p, (MJ/cm^3)$^{1/2}$] and hydrogen-bonding ability [δ_h, (MJ/cm^3)$^{1/2}$] [27]. The HSPs (δ_d, δ_p, δ_h) about miscellaneous solvents and targeted compounds were theoretically calculated from Group Contributions according to Hoftyzer and Van Krevelen method [28,29]. The calculated methods were shown in the following equations (2), (3), and (4). Eq. (5) was used to calculate the solubility parameters for mixed solvents. The HSPs results were expressed as Tears Trigonometric Graph and their calculation methods were based on Eqs. (6), (7), and (8):

Table 1
Types, compositions, Hansen solubility parameters and properties of various sustainable solvents.

Coding	Solvent type		Composition 1	Molar ratio of composition 1 to choline chloride	Aqueous volume fraction	δ_d (MJ/m^3)$^{1/2}$	δ_p (MJ/m^3)$^{1/2}$	δ_h (MJ/m^3)$^{1/2}$	Density Kg/m^3	Surface tension N/m	Viscosity Pa·s	Acoustic velocity m/s	Specific heat capacity (J/kg·°C)
DES1	Deep eutectic solvents	alcohol	Glycerol	2:1	30%	16.8	10.4	23.8	1139	0.065	0.0111	1234	2704
DES2			1,2-Propanediol	2:1	30%	16.4	8.6	19.8	1063	0.045	0.0098	1046	932
DES3			1,4-Butanediol	2:1	30%	16.3	12.5	18.7	1043	0.050	0.0105	1121	967
DES4			Ethylene glycol	2:1	30%	16.6	9.6	19.6	1097	0.049	0.0064	1078	804
DES5		acid	Citric acid	2:1	30%	15.9	7.0	17.6	1232	0.054	0.0166	1067	1178
DES6			Malic acid	2:1	30%	17.5	7.7	18.5	1205	0.063	0.0096	1176	108
DES7			Lactic acid	2:1	30%	17.3	8.7	20.7	1106	0.044	0.0073	1011	919
DES8		sugar	Sucrose	1:1	30%	16.6	13.5	13.3	1242	0.066	0.0389	1187	679
DES9			Glucose	1:1	30%	15.2	10.1	22.2	1186	0.072	0.0135	1277	508
DES10		amine	Urea	2:1	30%	20.5	12.2	18.4	1103	0.073	0.0034	1339	1097
SOL1	Organic	–	Methanol	–	40%	15.3	13.0	26.3	892	0.035	0.0019	1003	3078
SOL2	Water	–	Water	–	100%	15.5	16.0	42.3	1000	0.071	0.0017	1393	4200
SOL3	Bio-based solvent	–	Ethanol	–	40%	15.7	10.2	24.0	899	0.028	0.0023	883	3014
SOL4		–	Ethyl lactate	–	40%	15.9	9.3	18.5	1021	0.031	0.0031	871	2639
SOL5		–	Ethylene glycol	–	40%	17.0	11.0	26.0	1080	0.054	0.0044	1147	2864
SOL6		–	Glycerol	–	40%	17.4	12.1	29.3	1163	0.065	0.0147	1220	2864
SOL7	Polyethyleneglycol	–	Polyethylene glycol 200	–	40%	16.8	10.1	8.8	1069	0.048	0.0113	1081	2754
SOL8		–	Polyethylene glycol 400	–	40%	16.8	10.1	8.8	1090	0.047	0.0217	1057	2743
SOL9		–	Polyethylene glycol 600	–	40%	16.8	10.1	8.8	1078	0.049	0.0285	1088	2749

$$\delta_d = \frac{\sum F_{di}}{V_m} \tag{2}$$

$$\delta_p = \frac{\sqrt{\sum F_{pi}^2}}{V_m} \tag{3}$$

$$\delta_h = \sqrt{\frac{\Sigma E_{hi}}{V_m}} \tag{4}$$

$$\delta_I = x_1\delta_{i,1} + x_2\delta_{i,2} + x_3\delta_{i,3} \tag{5}$$

$$f_d = \frac{\delta_d}{\delta_d + \delta_p + \delta_h} \tag{6}$$

$$f_p = \frac{\delta_p}{\delta_d + \delta_p + \delta_h} \tag{7}$$

$$f_h = \frac{\delta_h}{\delta_d + \delta_p + \delta_h} \tag{8}$$

where F_{di}((MJ/m^3)$^{1/2}$·mol^{-1}), F_{pi} ((MJ/m^3)$^{1/2}$·mol^{-1}), and E_{hi} (J/mol) respectively correspond to the group contributions of dispersion forces, dipole force and hydrogen-bonding [29]. V_m is the molar volume (cm^3/mol). x_1, x_2, and x_3 are the mole fraction of each solvent in the mixed solution. The subscript i represents d, p, or h.

2.6. Numerical simulation of bubble dynamics

To obtain the bubble behavior in various neoteric solvents, Rayleigh-Plesset bubble dynamics were introduced since it considered the impacts of liquid density, viscosity, and surface tension on the bubble lifetime [30].

$$R = \frac{\left[\frac{1}{\rho_L}P_g(R,t) - P_0 - P_a(t)\right] + \frac{R}{\rho_L C_L}\frac{d}{dt}\left[\frac{1}{\rho_L}P_g(R,t) - P_a(t)\right] - \frac{4\mu}{\rho_L}\frac{\dot{R}}{R} - \frac{2\sigma}{R\rho_L} - \frac{3}{2}\left(\dot{R}\right)^2}{\ddot{R}} \tag{9}$$

$$P_g(R,t) = (P_0 + \frac{2\sigma}{R_0} - Pv)(\frac{R_0^3}{R^3})k \tag{10}$$

$$P = P_m(\frac{R}{R_{min}})^{3k} \tag{11}$$

where R is the evolution of bubble radius with time. $\dot{R}$ is the first derivative of R that means the speed of bubble wall. $\ddot{R}$ is the second derivative of R, which means acceleration speed of bubble wall. R_0 is the ambient bubble radius. P_g (R,t) is the pressure inside the bubbles. P_0 is the ambient pressure (1.0 atm). $P_a(t)$ is driving pressure of ultrasound (1.4 atm). ρ_L is the liquid density (Kg/m^3). C_L is the speed of the ultrasonic wave (m/s). μ is liquid viscosity (Pa·s). σ is the surface tension of solvent (mN/m). P_v is the vapor pressure inside the bubble (1.2 atm). k is the polytropic exponent (considering the isothermal assumption during the bubble lifetime, k = 1). R_{min} is the minimum bubble radius during the period. The equation was solved by the fourth-fifth order Runge-Kutta algorithm.

2.7. Visualization of cavitational activity by sonochemiluminescence

Luminol molecules can react with radical species that have strong oxidizability and electronic capture capability, and further trigger the formation of unstable amino phthalate derivatives in an excited state. When the excited state jump into the ground state, excess energy will be emitted as visible bluish light. Thus, the light luminance can reflect the spatial distribution and the number of radical species [31]. 0.1 g/L luminol solutions and 1 g/L NaOH solution were used and the operating parameters were the same as above extraction parameters. The images

were collected using a digital camera (Nikon D90) in a completely dark room. The specific parameters were as follows: exposure time 30 s, exposure compensation +2, aperture 5.6, ISO 1250, focal distance 58 mm.

2.8. Observation of ultrasound-induced modification

Untreated orange peels were observed by a stereomicroscope (Leica M205A) to obtain the main structural features. At the same time, to identify whether or not the cell structures of epidermis were damaged, the peels after ultrasonic treatment were stained 5 min by Sudan red dye and then were observed under a microscope (Olympus BX43).

2.9. Ultrastructural observation of Scanning Electron Microscope

To further evaluate the sono-aggressiveness on the orange peels at the microscopic level in different solvents, identical operating procedures same as the above extraction methods were performed in treated peels (1 cm^2) but the untreated peels were not radiated by ultrasound. The ultrastructural modifications were analyzed by Scanning Electron Microscope (SEM, Phenom Pro10102). All samples were dehydrated 15 min in different aqueous ethanol concentration (20%, 40%, 60%, 80%, 90%, and 100%) and fixed 15 min in 2% glutaraldehyde phosphate buffer (pH = 7.0). After that, all samples were dried and then sprayed with gold for SEM analysis.

2.10. Monitoring the individual phenolic acids

Since bound phenolic acids dominate the majority in orange peel and need to be hydrolyzed before HPLC analysis. 5 mL NaOH solutions (4 mol/L) were added into the 5 mL extraction solutions and then hydrolyzed in dark for 4 h. Then the pH was adjusted to 2 with 6 mol/L HCl. 5 mL mixtures of ethyl acetate and diethyl ether (V:V = 1:1) were used to extract free phenolic acids three times and the extracts were evaporated by rotation. Finally using 60% aqueous methanol fixed the volume to 2 mL. The free phenolic acids including ferulic acid, sinapic acid, p-coumaric acid, p-hydroxybenzoic acid, vanillic acid, and caffeic acid were quantified by an Ultimate 3000 HPLC equipped with a DAD3000 and 250 × 4.6 mm × 5 μm ODS HYPERSIL C18 column (Thermo Scientific). Mobile phase: 100% methanol (A), 1% acetic acid (B). Elution procedure: 0–22 min, 20% A-80 %B; 22.1–38 min, 30 %A-70 %B; 38.1–48 min, 100 %A; 48.1–58 min, 20 %A-80 %B. Flow rate: 1 mL/min. Detection wavelength: 260 nm, 320 nm. Total phenolic acids yield (TPY) was defined by the following equation (Y_{TPY} μg/g):

$$Y_{TPY} = Y_{\text{ferulic acid}} + Y_{\text{sinapic acid}} + Y_{\text{p-coumaric acid}} + Y_{\text{p-hydroxybenzoic acid}} + Y_{\text{vanillic acid}} + Y_{\text{caffeic acid}} \quad (12)$$

2.11. Monitoring the individual flavonoids

5 mL treated solutions were extracted three times with 5 mL ethyl acetate and then evaporated. Using 60% aqueous methanol fixed the volume to 2 mL. The individual flavonoids including hesperidin, nobiletin, didymin, narirutin, and sinensetin were quantified using an Ultimate 3000 HPLC equipped with a DAD3000 and 250 × 4.6 mm × 5 μm ODS HYPERSIL C18 column (Thermo Scientific). Mobile phase: 100% acetonitrile (A), 0.1% phosphoric acid (B), Elution procedure: 0–15 min, 20% A-80 %B; 15.1–35 min, 30 %A-70 %B; 35.1–45 min, 100 %A; 45.1–55 min, 20 %A-80 %B. Flow rate: 1 mL/min. Detection wavelength: 283 nm, 330 nm. Total flavonoids yield (TFY) was defined by the following equation (Y_{TFY} μg/g):

$$Y_{TFY} = Y_{\text{hesperidin}} + Y_{\text{nobiletin}} + Y_{\text{didymin}} + Y_{\text{narirutin}} + Y_{\text{sinensetin}} \quad (13)$$

2.12. DPPH radical scavenging activity

0.1 mol/L DPPH solution was prepared with methanol. 0.5 mL samples and 1.5 mL DPPH solutions were mixed with a pipette gun. 0.5 mL methanol solutions and 1.5 mL DPPH solutions were mixed as blank control. The mixtures were incubated for 10 min and then the absorbances were measured at 517 nm with an ultraviolet spectrophotometer. The DPPH radical scavenging capacity was calculated according to Eq. (14):

$$DPPH\ \ radical\ \ scavenging\ \ capacity\ (\%) = \left(A_{\text{control}} - A_{\text{sample}}\right)/A_{\text{control}} \times 100 \quad (14)$$

2.13. ABTS radical scavenging activity

2.45 mmol/L potassium persulfate solution and 7 mmol/L ABTS solution were mixed (V: V = 0.5:1) to react for 12–16 h in the dark. Using ethanol diluted the absorbance of the solution to 0.7 ± 0.02 to form a test reagent. 3.9 mL test reagents and 0.1 mL samples were mixed. At the same time, 3.9 mL ABTS solutions and 0.1 mL methanol were mixed as blank control. All mixtures were reacted for 10 min to measure the absorbance at 734 nm. The ABTS radical scavenging capacity (%) was calculated according to equation (15):

$$ABTS\ \ radical\ \ scavenging\ \ capacity(\%) = \left(A_{\text{control}} - A_{\text{sample}}\right)/A_{\text{control}} \times 100 \quad (15)$$

2.14. Ferric-ion reducing antioxidant power assay (FRAP)

The FRAP working solutions containing 0.1 mol/L acetic acid buffer (pH = 3.6), 10 mmol/L TPTZ solutions (dissolved with 40 mmol/L hydrochloric acids), and 20 mmol/L ferric chloride were prepared (V: V: V = 10:1:1). 0.1 mL samples and 2.45 mL working solutions were mixed. The blank control was 0.1 mL methanol and 2.45 mL working solutions. The dark reaction lasted for 30 min. The maximum absorbance value was measured by a UV spectrophotometer at 593 nm. The results were expressed as mg Trolox equivalent/g. The standard curve was Y = 22.27X-0.0982 (X is the absorbance and Y is the Trolox equivalent mg).

2.15. Statistical analysis

All data were subjected to the one-way ANOVA analysis and Duncan's multiple tests to distinguish significant differences. All correlation analyses were performed by Pearson's correlation coefficient. The statistical significance of $P < 0.05$ was considered. All procedures were carried out in triplicate.

3. Results

3.1. Simulation and verification of cavitation bubbles

The impacts of both effects of ultrasound on the biorefinery mainly involve two facets encompassing the impact of physical effects on the extraction yield and the impact of chemical effects on the degradation of targeted components. Physical effects such as shear forces, microjets, and shock waves mainly originate from bubble collapse that contributes to the disintegration of plant materials. However, the collapsing aggressiveness is determined by bubble dynamics in particular maximum bubble radius (MBR) but MBR is extremely susceptible to the intrinsic properties of the used solvents [32]. We hypothesized that the solvent properties can control the collapsing intensity of bubbles and harness the disintegration of raw materials by handling the dimension of cavitational bubble and further determine the releasing rate of biocompounds. Hitherto, obtaining MBR is a tremendous challenge in a general laboratory as the bubble lifetime is at the magnitude of

microsecond [33]. Therefore, to resolve this predicament, related parameters of MBR were numerically simulated in multifarious solvents. The evolutionary results of bubble radius (**a**) and collapsing pressure (**b**) were illustrated in Fig. 1. For most of the solvents, as the sound pressure changed from compression to rarefaction, the bubbles began to grow swiftly and collapse at about 1/2 bubble lifetime. Those bubbles with larger size underwent several damped oscillations after the initial collapse and generated more small bubbles as the source of cavities in the next cavitation cycle. An increase in the MBR induced a substantial increase in the volume compression ratio $(R_{max}/R_0)^3$, which more tended to generate higher collapsing pressure. Meanwhile, it could be highlighted that those solvents possessed common properties with low viscosity, low density, and low surface tension. An increase in the viscosity needing more energy to surmount the intermolecular forces from surrounding liquids and giving rise to an increase in surface stability limits the nucleation and cavitation [18]. Thus, the low-viscosity solvent has a disposition to generate a large-dimension bubble, which is responsible to the high cavitational intensity. In support of this hypothesis, aqueous polyethylene glycol (PEG) had an increase in the viscosity from PEG 200 to PEG600 due to the extension of molecular chain resulting in a decrease in MBR (26.2, 19.8, 16.8 μm). Also, from our results of correlations between solvent properties and MBR (Table 2), we found that correlation strength was arranged in the following order: viscosity (−0.86**) > density (−0.83**) > surface tension (−0.64**). To verify whether or not cavitational bubbles with different dimensions at collapse caused the different damage on the material surface, microscopic imaging technologies were introduced to observe the surface modifications. Preferentially, the stereomicroscope showed that the epidermal structure of the oil gland had a looser filamentous structure (Fig. 2**A**). Subsequently, using Sudan red dye to stain the peel without (Fig. 2**B**) and with (Fig. 2**C**) ultrasonic treatment found that only those cells surrounding the oil gland with ultrasonic treatment were destroyed (only the non-intact cells can be stained) and other cells were integral without any damage, which indicated that ultrasonic effects were closely dependent on the tissue texture and/or cell structure. Cavities or microbubbles first penetrate the oil glands and these as a source of the collapsing bubble will undergo compression and rarefaction phase driven by sound pressure finally experiencing catastrophically imploding and fragmenting process. Therefore, the physical damage will be first observed from the oil glands. The reason for heterogeneous damage may be attributed to the theory that is selective effects and/or ordering effects, which was first proposed by Vinatoru [34]. Consistent with our results, Khadhraoui et al. [35] also found that

Table 2
The correlations between solvent properties and maximum bubble radius (MBR).

-	Solvent properties		
-	Viscosity	Density	Surface tension
MBR	−0.86**	−0.83**	−0.64**

** represents the significance of $P < 0.01$.

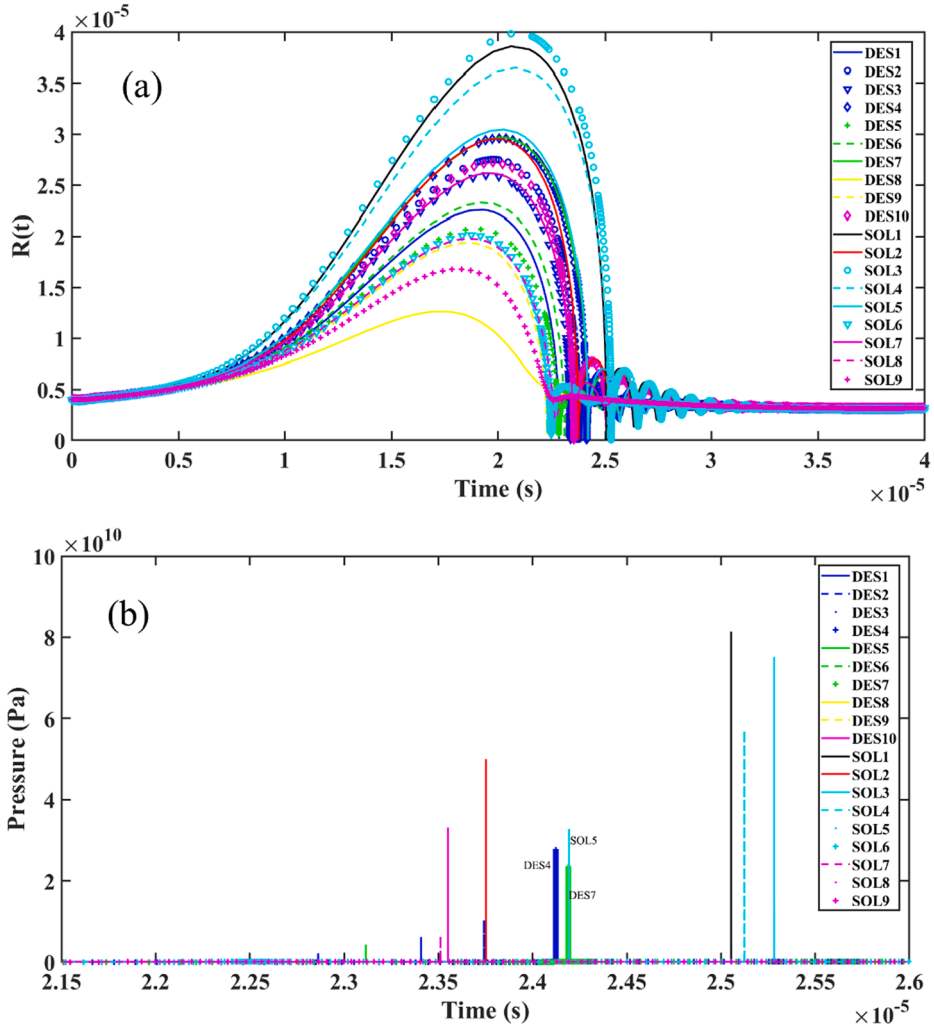

Fig. 1. Bubble radius (a) and collapsing pressure (b) regarding the time evolution. R(t) is the evolution of the bubble radius with time.

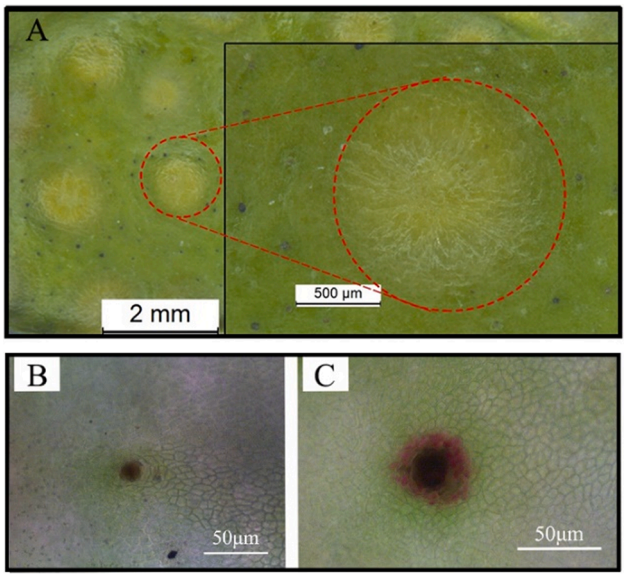

Fig. 2. Stereomicroscopic observation of the structure of oil glands (A) and microscopic observation of the oil gland stained by Sudan red without (B) and with (C) 20 min ultrasound treatment. (For interpretation of the references to colour in this figure legend, the reader is referred to the web version of this article.)

some of the local tissues kept intact but other tissues with long and branched structures were completely deformed or removed on the non-glandular trichomes of rosemary leaves, which further demonstrated the ordering effects including erosion, shear forces, sonoporation, fragmentation, capillary effect, and detexturation. To observe the influence of acoustic cavitation more intuitively on tissue structures, micromorphological observations by SEM were carried out and US-induced pronounced destruction can be observed clearly around the oil gland (Fig. 3). For control check (CK) without ultrasound, the surfaces and surroundings of the oil gland were smooth and complete. However, for the DES7, SOL1, and SOL4, the oil glands generating a myriad of debris on their surface indicated that one may be spoiled by mechanical forces. Concomitantly, for DES10 and SOL2 with a high and approximate collapsing pressure based on the bubble kinetics, a noticeable crack can be observed on the oil gland, which may be ultrasound-induced remarkable microjets or shear forces. Also, no significant structural modifications can be noticed after ultrasound treatment in DES8. The data regarding the maximum collapsing pressure calculated by Rayleigh-Plesset equation showed that DES8 had a second-lowest collapsing pressure. However, the generating energy may be not enough to destroy the oil glands even with a subtle modification. In another pioneering study, Majumdar and co-workers [15] designed an ingenious iodometry to measure the impacts of organic solvents immiscible with water on the attenuation coefficient and cavitation activity and obtained analogous results that viscosity, density and surface tension were not individually but synthetically impact the cavitational intensity. Unfortunately, this methodology was inappropriate for those solvents that were miscible with water whereas our results through stimulating bubble behaviours provided a high-feasibility channel and original insight to resolve the nondeterminacy of acoustic cavitation. In addition, the reliability of using this methodology to predict sono-recovery yield will be explained later because there exists an issue needing to be clarified imminently.

3.2. Compatibility between solvent system and targeted compounds

Although ultrasound can induce the catastrophic fragmentation on the surfaces of raw materials, enhance the accessibility between solvents and solutes, and partly improve the solubilization of targeted compounds [36,37], if further improvement in the production of targeted compounds wants to be achieved, solvent affinity towards targeted compounds should be considered. In this regard, Hansen solubility parameters (HSPs) are one of the effective approaches to acquire basic information about compatibility [38]. Moreover, a faced reality to be surmounted is that approximately 1000 HSPs data were overt and have been successfully employed in some commercial fields [38] but there were no reference publications for the HSPs about 11 kinds of health-related value-added compounds and thereby they were calculated in Table 3. The compatibility was visualized by using Teas triangle graph (a close distance between two symbols means strong compatibility) [39] and shown in Fig. 4. Notably, SOL2 (pure water) presented bad compatibility regardless of phenolic acids and flavonoids. Concordant with well previous findings, Kantar et al. [21] once obtained that solubility of naringin in pure water was relatively poor but choline chloride-based DESs authorized the excellent solubility. Therefore, this is one of the reasons why water as a solvent in the maceration extraction cannot achieve a relatively satisfactory recovery result [40]. Furthermore, we can divide these solvents into four categories: best score (DES2, DES4, DES5, DES6, DES7, and DES10), better score (DES1, DES3, DES8, DES9, SOL4, SOL7, SOL8, and SOL9), good score (SOL1, SOL3, SOL5, and SOL6) and bad score (SOL2). In support of this classification, Brás and coworkers [41] using relative energy difference (RED, low RED represents high dissolving ability) to express HSPs obtained similar results where high compatibility (RED < 1), moderate compatibility ($1 <$ RED < 3) and poor compatibility for cynaropicrin respectively existed ethyl acetate (better score), ethanol/water (good score) and water (bad score). Nevertheless, although the performance of the bulk of deep eutectic solvents seemed to manifest the best compatibility than other neoteric solvents (for example, DES5, DES6, and DES10 have excellent solubility for phenolic acids, especially caffeic acid and flavonoids comprising narirutin, hesperidin and didymin due to their similar structure with C6-C3-C6 carbon skeleton and glycoside from Fig. 5), in realistic recovery procedures, the situation is not necessarily so and this paradox will be discussed later.

3.3. Radicals-generating ability visualized by sonochemiluminescence

In addition to the aforementioned factors to affect the recovery production, a non-ignorable truth is that chemical effects are always along with the occurrence of ultrasound and mediate free radicals that are capable of inducing secondary redox reactions and further causing the degradation or deterioration of the value-added compounds [24,42,43]. As mentioned in section 2.7, sonochemiluminescence (SCL) can characterize the radicals-generating ability. If a solvent presents a low SCL signal, we can think that this solvent can eliminate or inhibit the formation of free radicals to some extent and further play a role to protect targeted compounds [44]. Therefore, we examined the SCL to ascertain whether or not it can impact the accuracy of bubble model. For the visible SCL from Fig. 6**a**, in terms of the spatial distribution of cavitation-activity zone, the strongest SCL luminosity emerged preferentially in the vicinity of ultrasonic horn tip and axial direction, which indicated that the concentration of free radicals and the active bubbles were unevenly distributed. Those bubbles near the transducer had a higher core temperature after collapse to release more free radicals and then diffused from the axial proximal end towards the distal axis. The relatively strong signal of SCL can be observed in the long-chain alcohol solvents such as DES2 (1,2 propanediol/water) and DES4 (ethylene glycol/water). But short-chain alcohol solvents such as SOL1 (methanol/water) and SOL4 (ethanol/water) appeared completely quenching SCL (Fig. 6**b**). The reason may be that excessive alcohol molecules adsorbed at the gas-liquid interface resulting in the injection of alcohol into the bubble to weaken the collapsing intensity [45]. Meanwhile, the presence of alcohol molecules can inhibit the bubble coalescence and limit the formation of large bubbles further confining the volume

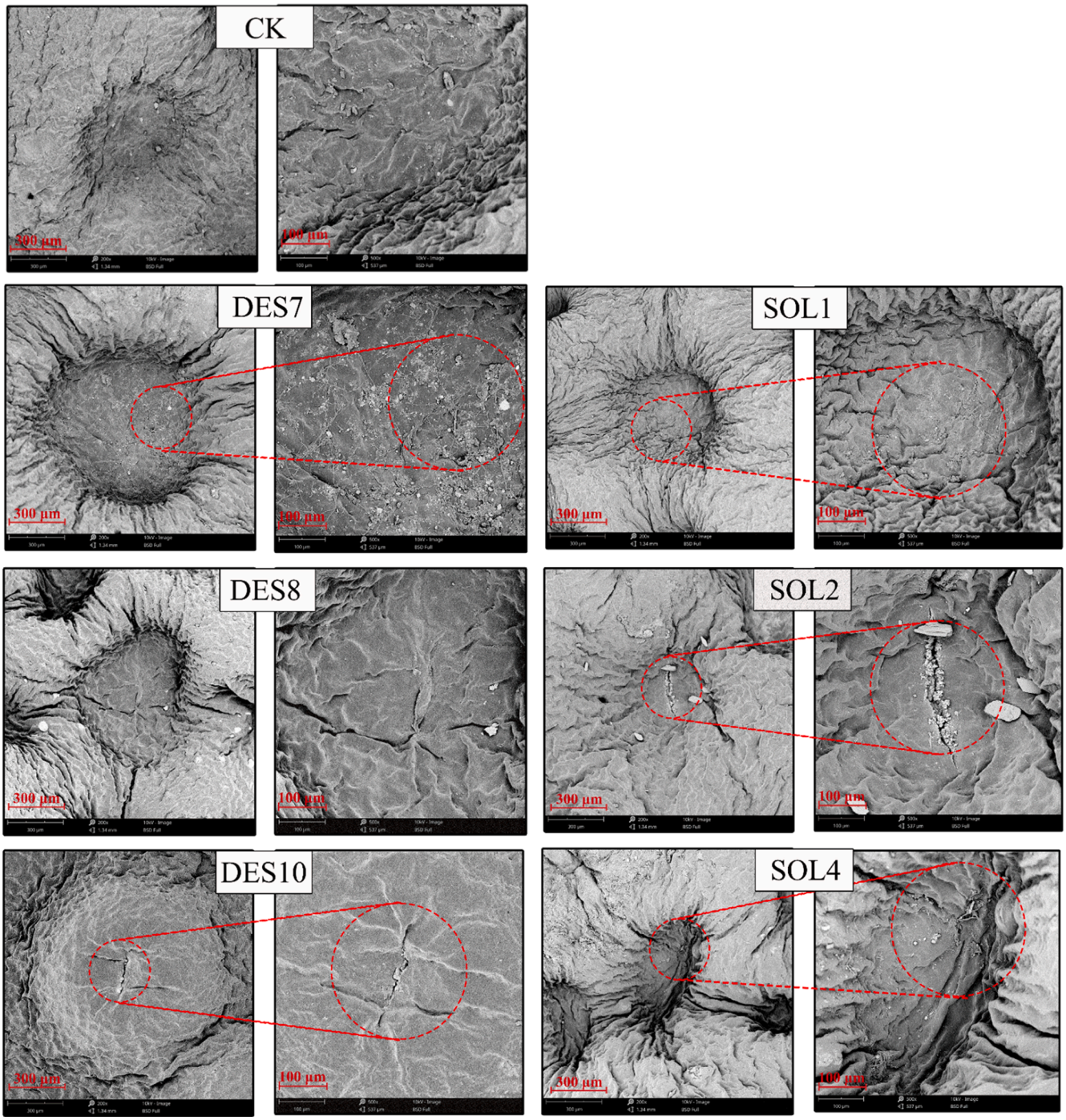

Fig. 3. Ultrastructural observation of oil gland by Scanning Electron Microscope.

compression ratio [46]. Inconsistent with our results, several authors found that attenuation intensity of sonoluminescence signal increased with the increase of chain length in alcohol, n-alkyl carboxylic acids, and amines solution [47–49]. This divergence could be attributed to the postulate that choline chloride may have an indispensable contribution to SCL enhancement. For instance, in stark contrast to DES1 containing choline chloride (glycerol/choline chloride), the SCL in SOL6 (glycerol) was completely quenched (Fig. 6**b**). The existence of choline chloride will form hydrogen bonds with polyhydroxy alcohol molecules. If an alcohol molecule needs to enter the bubble, it must overcome the hydrogen bond force between the choline chloride and glycerol. Therefore, due to the limitation of energy, the concentration of alcohol molecules inside the bubble was at a low-level giving rise to the enhancement of SCL in DES1. Also, no significant SCL signal was observed from these solvents including DES6, SES7, DES8, and SOL4. No signal for DES8 may be that the highly viscous property as the main factor hinders the bubble to grow to an active size and limits the collapsing temperature at this level of driving sound pressure [50]. On the other hand, the increment of viscosity leads to the increase of the cavitation threshold, which may reduce the number of active bubbles and further weaken the SCL luminosity. As for DES6 and DES7, a low-pH solution provided by malic acid and lactic acid given rise to the quenching SCL, which was in accordance with the previous investigation in n-alkyl carboxylic acids [47]. From these available results, we found that SCL was extremely susceptible and easily affected by exogenous factors especially the discrepancy of the prescription of neoteric

Table 3
Hansen solubility parameters for each phenolic acid and flavonoid.

Polyphenols	δ_d (MJ/m^3)$^{1/2}$	δ_p (MJ/m^3)$^{1/2}$	δ_h (MJ/m^3)$^{1/2}$
Ferulic acid	20.9	5.7	14.2
Sinapic acid	20.5	6.0	13.8
p-coumaric acid	21.4	6.2	14.7
p-hydroxybenzoic acid	18.9	3.4	14.4
Vanillic acid	18.8	3.9	13.8
Caffeic acid	22.1	6.3	17.8
Hesperidin	26.6	7.2	16.7
Nobiletin	18.7	6.7	9.7
Didymin	25.8	7.0	15.1
Narirutin	26.8	7.3	16.9
Sinensetin	23.6	7.6	10.8

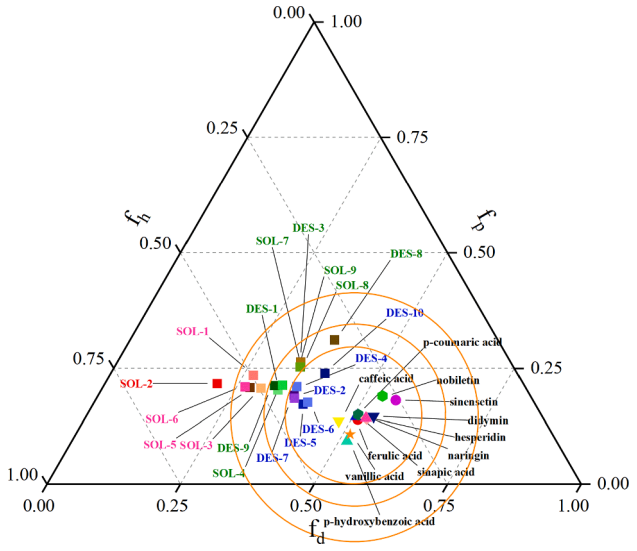

Fig. 4. Hansen solubility parameters visualized by Teas triangle graph.

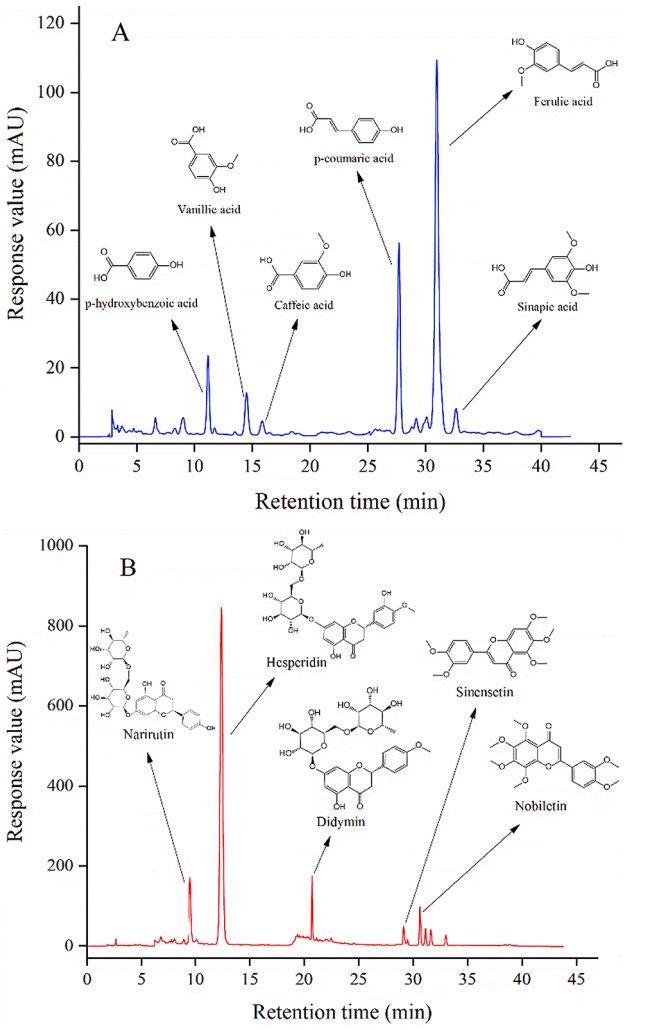

Fig. 5. The retention time and chemical structure of six phenolic acids (A) and five flavonoids (B).

solvents, which tremendously determined the radicals-generating ability. But whether the equivalent of these free radicals can affect our targeted compounds will be discussed later. The only information we can obtain was that DES6、DES7、DES8、DES9、SOL1、SOL4 and SOL6 possessed optimal protection of native activity for all value-added compounds due to their extremely weak or completely quenching SCL.

4. Discussion

Previously, the solubility profiles of various sustainable solvents and the impacts of their intrinsic properties on the cavitational characteristics were comprehensively analysed. Subsequently, we aimed to elucidate the causality or synergy between the aforementioned latency and recovery results. The yield for six phenolic acids and five flavonoids was quantified by HPLC (Fig. 5, Fig. 7). In addition to DES1, DES5, and DES6, the extraction yield of phenolic acids in the majority of solvents presented a small fluctuating trend (24.3–30.2 μg/g). But for flavonoids, only three solvents comprising SOL1, SOL3, and SOL4 possessed outstanding performances (175.2–247.7 μg/g). Aberrantly, partial solvents showed excellent HSPs but did not perform corresponding extractability. In the case of DES5 and DES6, prominent HSPs did not achieve satisfactory recovery efficiency regardless of the phenolic acids (21.5 and 12.5 μg/g) or the flavonoids (46.8 and 54.9 μg/g) (Fig. 7). For one thing, the physical properties of solvent after ultrasonically treated raw materials and the varying chemical compositions affect the interplay and molecular bonding in turn impacts the recovery efficiency. For another, the reason for this gap may be that the extraction process involves material crushing, solvent permeation, solute exudation, and the solubility of targeted compounds in the targeted solvent, whereas HSPs only can be used to predict the solubility but not the mass transfer and diffusion kinetics [21,51]. Therefore, using HSPs only to predict the solubility of solutes in miscellaneous solvents may be feasible, but for the recovery process, it is necessary to simultaneously consider the cavitational characteristics and HSPs. In all tested solvents, a noticeable phenomenon can be seen that top three MBR (39.8, 38.6, and 36.5 μm) appeared in ethanol/water (SOL3), methanol/water (SOL1), and ethyl lactate/water (SOL4) (Fig. 1), and corresponding extraction yield in phenolic acids (28.6, 27.8 and 27.8 μg/g) and flavonoids (245.1, 175.2 and 247.7 μg/g) also exhibited relatively high value. Similarly, PEG 200 to PEG600 due to their decreasing MBR induced further dwindle in extraction yield for phenolic acids (30.2 to 27.2 to 24.3 μg/g) and flavonoids (66.6 to 52.6 to 39.7 μg/g). Strangely, DES8 with the second-lowest MBR just for flavonoids presented a relatively low yield (22.0 μg/g). Meanwhile, an intriguing thing that needed to be noticed was phenolic acids and flavonoids having totally different trends in yield. This also can be highlighted from the correlation data between MBR and extraction yield (phenolic acids and flavonoids), and the results presented a statistically significant high correlation for flavonoids (0.75**) but not for phenolic acids (0.33) (Table 4), which may be the heterogeneous distribution in-situ. Commonly, citrus peel consists of flavedo layers and albedo layers and the former present yellow colour embellished by oil glands and the texture was more fragile, but the latter exhibit white-colour inner spongy layer and accounts for more

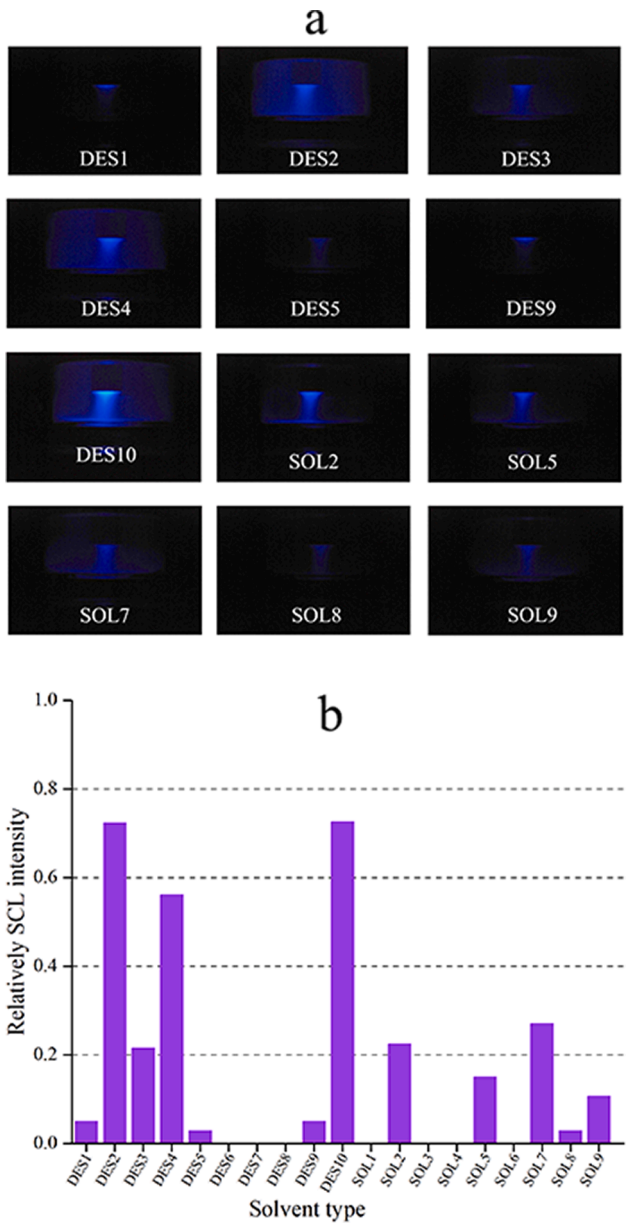

Fig. 6. Sonochemiluminescence (a) and relative SCL intensity (b) in various solvents.

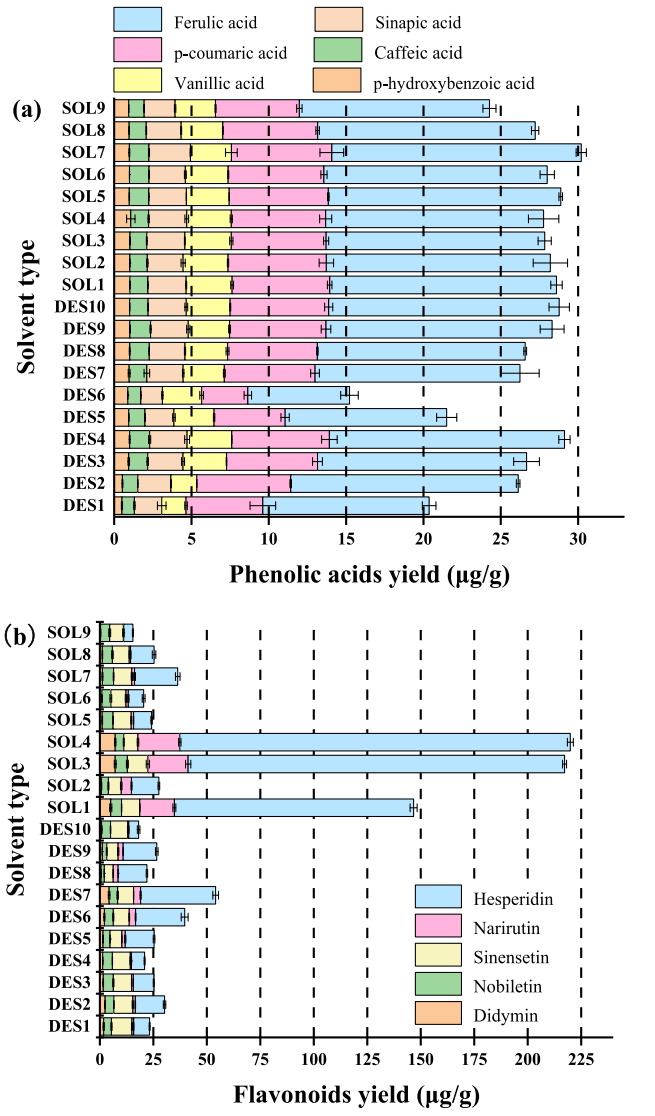

Fig. 7. The extraction yield of phenolic acids (a) and flavonoids (b) in various solvents.

Table 4
The correlations between solvent properties, MBR and total phenolic acids yield (TPY), total flavonoids yield (TFY).

Solvent properties	TPY	TFY
Viscosity	−0.20	−0.43
Density	−0.47**	−0.65**
Surface tension	−0.20	−0.74**
MBR	0.33	0.75**

** represents the significance of $P < 0.01$. No asterisk represents the nonsignificant correlation.

proportion than flavedo in citrus peels [52]. Between the flavedo and albedo forming a band about 40 μm thickness, most of the hesperidin is accumulated around the vascular bundles in the form of needle-shaped crystals [52]. Therefore, the recovery of flavonoids especially hesperidin needs to deeply destroy the tissues of the plant material first and then rely on the affinity of the solvent system to bring the solute molecules into the bulk solvent. As for phenolic acid, whose location mainly exists in the albedo layer that is fragile [53]. Hence, the recovery of phenolic acids and flavonoids may present different sequences and mechanisms in the extraction. Besides, considering the statements about SCL, the only information we can ascertain was which solvents possessed the lowest radical-generating capacity but unexpectedly, the SCL luminosity and the yield (caffeic acid, 0.65**; p-coumaric acid, 0.53* and narirutin, −0.51*) showed some positive or negative correlations, which seemed that SCL contributed to the extraction of the two phenolic acids, but not conducive to the extraction of narirutin. In our previous study [24] caffeic acid had higher sonochemical stability than rutin and cyanidin-3-glucoside. Thus, the correlational discrepancy may be that narirutin as a flavonoid have a high disposition to degrade than caffeic acid and p-coumaric acid. Consistent with this result, for DES4 and DES7 with the prerequisite of similar MBR and HSPs, DES4 achieving unsatisfactory extraction yield in flavonoids as compared to DES7 may be attributed to the SCL that an extremely strong signal in DES4 means more production of free radicals. Regarding bio-based SOL4, although it has a relatively poor affinity, the synergistic effect between the high collapsing pressure inducing the local tissue destruction and the completely quenching SCL determines the excellent extractability. In addition, considering the huge difference in radicals-generating capability and the dose-response

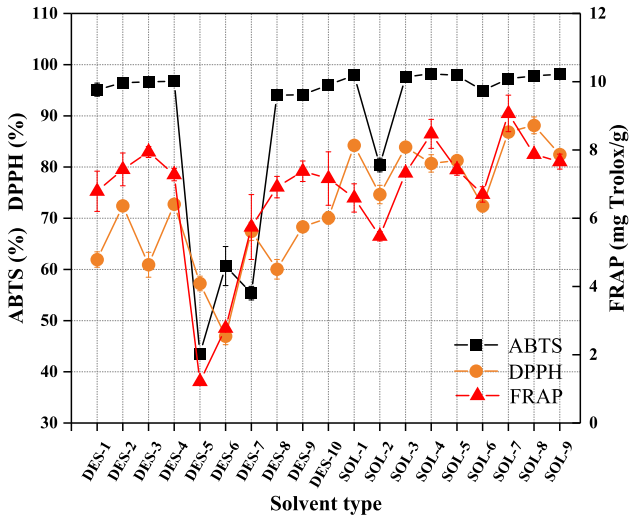

Fig. 8. Antioxidant capacity of extracts evaluated by DPPH, ABTS and FRAP in various solvents.

Table 5
The correlations among phenolic acids, flavonoids, phenolic acids & flavonoids, DPPH, ABTS, FRAP and SCL.

Extraction yields (μg/g)	ABTS	DPPH	FRAP	SCL
Ferulic acid	0.718**	0.729**	0.624**	0.649**
p-coumaric acid	0.722**	0.727**	0.625**	0.533*
p-hydroxybenzoic acid	0.301	0.073	0.002	−0.145
Vanillic acid	0.300	0.064	0.040	0.087
Caffeic acid	0.333	0.431	0.328	0.173
Sinapic acid	0.674**	0.670**	0.517*	0.194
Phenolic acids	0.579**	0.711**	0.688**	0.458*
Hesperidin	0.308	0.172	0.154	−0.440
Nobiletin	0.534*	0.269	0.244	0.313
Didymin	0.261	0.095	0.005	−0.243
Narirutin	0.356	0.117	0.143	−0.513*
Sinensetin	0.301	0.322	0.331	0.387
Flavonoids	0.159	0.376	0.175	−0.301
Phenolic acids & Flavonoids	0.190	0.412	0.211	−0.137

* and ** represent the significance of $P < 0.05$ and $P < 0.01$, respectively. No asterisk represents the nonsignificant correlation. Phenolic acids & Flavonoids means the sum of all individual phenolic acid and individual flavonoid.

relationship [24] the native activity of value-added compounds through the total antioxidant activity (TAA) including DPPH, FRAP, and ABTS (Fig. 8) and the correlations between extraction yield and TAA were analysed (Table 5). Somewhat counterintuitively, phenolic acids especially p-hydroxybenzoic acid (0.72**), ferulic acid (0.72**) and sinapic acid (0.67**) contributed overwhelmingly to the TAA in ABTS (0.58**), DPPH (0.71**) and FRAP (0.69**) but flavonoids (except nobiletin, 0.53*), phenolic acids & flavonoids, ABTS, DPPH and FRAP showed barely significant correlations (Table 5). In the case of DES7 and DES8 with equal phenolic acid yield and completely quenching SCL, high flavonoids yield in DES7 didn't produce higher TAA than that of DES8, which may be attributed to the solvent dependence, that is, thermodynamically preferred mechanism including hydrogen atom transfer, single electron transfer followed by proton transfer and sequential proton loss electron transfer [54]. Moreover, it was predicted that SCL luminance can reversely mirror the native activity due to the radicals-attacking pathway but out of the blue there were neither positively nor negatively significant correlations. DES9 and SOL2 had equal yield in phenolic acids and flavonoids but stronger SCL in SOL2 resulted in the weakened TAA. Undeniably, some of the solvents such as DES 10 having brighter SCL didn't seem to produce significant impacts on TAA compared to SOL6. Therefore, we couldn't say that free radicals mediated by ultrasound basically generated no impacts on the value-added compounds but the presentation of the very weak correlations suggested to some extent that SCL had a limited effect on the quality and quantity of the value-added compounds. As predicted by above results, ethyl lactate outperformed other solvents both in terms of phenolic compounds yield and antioxidant potential in the extracts and presented excellent potential. Thus, MBR can be considered as a decision-making tool to predictive the final flavonoids yield.

5. Conclusions

The sustainable recovery process has become a focus in process systems engineering aiming at the transition from a petroleum-based refinery to a green- or bio-refinery while guaranteeing a safe quality and high quantity of value-added compounds for the sake of productivity and commercialization. Nevertheless, although developed sustainable solvents were recognized as safety and sustainability, how their intrinsic properties affect the recovery process under the ultrasonic field exists an enormous challenge. From the point of view of the interaction between ultrasound and solvent specificity, the results revealed that the maximum bubble radius (MBR) driven by ultrasound was the most decisive parameter to predict the recovery of flavonoids ($r = 0.75$**). Meanwhile, the SEM characterizations demonstrated that varying MBR in different solvents induced various destruction to citrus peels. Besides, microscopic examination demonstrated that the selective destruction of ultrasound preferentially began with the oil gland structures. Also, this work demonstrated that employing Hansen solubility parameters to predict solvent extraction capability in an ultrasonic environment was unreliable since the solvent infiltration and solute exudation also depended on the cavitational intensity. Sonochemiluminescence (SCL) signal existing prodigious discrepancy revealed the discrimination of radical-generating ability of neoteric solvent but this had a limited effect on the end-use quality and quantity of value-added compounds. Finally, aqueous ethyl lactate had paramountcy in all candidates and that has been confirmed to be the most promising sustainable solvents due to the relatively high collapsing pressure, completely quenching SCL and superior native activity. This study demonstrated the limitation of HSPs in screening sustainable solvents and proposed a new insight to address a common conundrum caused by the intrinsic properties of sustainable solvents that can limit practical applications involving the mass transfer process. With the continuous discovery of sustainable solvents and characterization of their intrinsic properties, employing this theoretical prediction will contribute to achieving an outstanding process control and prediction.

CRediT authorship contribution statement

Pengxu Wang: Conceptualization, Methodology, Validation, Formal analysis, Software, Investigation, Data curation, Writing - original draft, Writing - review & editing, Project administration. **Yaqin Ma:** Conceptualization, Validation, Investigation, Data curation, Writing - review & editing, Project administration, Funding acquisition, Supervision. **Chen Zhang:** Investigation, Resources, Writing - review & editing, Formal analysis. **Meng Jia:** Software, Investigation, Writing - review & editing.

Declaration of Competing Interest

The authors declare that they have no known competing financial interests or personal relationships that could have appeared to influence the work reported in this paper.

Acknowledgments

This study was supported by The Modern Agricultural (Citrus) Technology System of China (CARS-26-06B) and Fundamental Research Funds for the Central Universities (XDJK2019B048).

References

[1] UN, Transforming Our World: the 2030 Agenda for Sustainable Development United Nations United Nations Transforming Our World: the 2030 Agenda for Sustainable Development. A/RES/70/1, 2015.

[2] S. Armenta, S. Garrigues, M. de la Guardia, Green analytical chemistry, TrAC - Trends Anal. Chem. 27 (2008) 497–511, https://doi.org/10.1016/j.trac.2008.05.003.

[3] B. Schuur, T. Brouwer, D. Smink, L.M.J. Sprakel, Green solvents for sustainable separation processes, Curr. Opin. Green Sustain. Chem. 18 (2019) 57–65, https://doi.org/10.1016/j.cogsc.2018.12.009.

[4] A. Grudniewska, J. Popłoński, Simple and green method for the extraction of xanthohumol from spent hops using deep eutectic solvents, Sep. Purif. Technol. 250 (2020) 117196, https://doi.org/10.1016/j.seppur.2020.117196.

[5] M. Koel, M. Kuhtinskaja, M. Vaher, Extraction of bioactive compounds from Catharanthus roseus and Vinca minor, Sep. Purif. Technol. 252 (2020) 117438, https://doi.org/10.1016/j.seppur.2020.117438.

[6] M.W. Nam, J. Zhao, M.S. Lee, J.H. Jeong, J. Lee, Enhanced extraction of bioactive natural products using tailor-made deep eutectic solvents: application to flavonoid extraction from Flos sophorae, Green Chem. 17 (2015) 1718–1727, https://doi.org/10.1039/c4gc01556h.

[7] Y. Gu, F. Jérôme, Bio-based solvents: an emerging generation of fluids for the design of eco-efficient processes in catalysis and organic chemistry, Chem. Soc. Rev. 42 (2013) 9550–9570, https://doi.org/10.1039/c3cs60241a.

[8] C.J. Clarke, W.C. Tu, O. Levers, A. Bröhl, J.P. Hallett, Green and sustainable solvents in chemical processes, Chem. Rev. (2018), https://doi.org/10.1021/acs.chemrev.7b00571.

[9] A. Leal Vieira Cubas, M. Medeiros Machado, R. Tayane Bianchet, K. Alexandra da Costa Hermann, J. Alexsander Bork, N. Angelo Debacher, E. Flores Lins, M. Maraschin, D. Sousa Coelho, E. Helena Siegel Moecke, Oil extraction from spent coffee grounds assisted by non-thermal plasma, Sep. Purif. Technol. 250 (2020) 117171. doi:https://doi.org/10.1016/j.seppur.2020.117171.

[10] J. Živković, K. Šavikin, T. Janković, N. Ćujić, N. Menković, Optimization of ultrasound-assisted extraction of polyphenolic compounds from pomegranate peel using response surface methodology, Sep. Purif. Technol. (2018), https://doi.org/10.1016/j.seppur.2017.11.032.

[11] H.S. Arruda, E.K. Silva, G.A. Pereira, C.F.F. Angolini, M.N. Eberlin, M.A. A. Meireles, G.M. Pastore, Effects of high-intensity ultrasound process parameters on the phenolic compounds recovery from araticum peel, Ultrason. Sonochem. 50 (2019) 82–95, https://doi.org/10.1016/j.ultsonch.2018.09.002.

[12] N.M. Peixoto Araujo, E.K. Silva, H.S. Arruda, D. Rodrigues de Morais, M. Angela A. Meireles, G.A. Pereira, G.M. Pastore, Recovering phenolic compounds from Eugenia calycina Cambess employing high-intensity ultrasound treatments: A comparison among its leaves, fruit pulp, and seed as promising sources of bioactive compounds, Sep. Purif. Technol. 272 (2021) 118920. doi:10.1016/j.seppur.2021.118920.

[13] M.M. Strieder, M.I.L. Neves, G.L. Zabot, E.K. Silva, M.A.A. Meireles, A techno-economic evaluation for the genipin recovery from Genipa americana L. employing non-thermal and thermal high-intensity ultrasound treatments, Sep. Purif. Technol. 258 (2021) 117978. doi:10.1016/j.seppur.2020.117978.

[14] Y. Tao, D.W. Sun, Enhancement of food processes by ultrasound: a review, Crit. Rev. Food Sci. Nutr. 55 (2015) 570–594, https://doi.org/10.1080/10408398.2012.667849.

[15] S. Majumdar, P.S. Kumar, A.B. Pandit, Effect of liquid-phase properties on ultrasound intensity and cavitational activity, Ultrason. Sonochem. 5 (1998) 113–118, https://doi.org/10.1016/S1350-4177(98)00019-4.

[16] E.L. Smith, A.P. Abbott, K.S. Ryder, Deep Eutectic Solvents (DESs) and Their Applications, 2014. doi:10.1021/cr300162p.

[17] P.R. Gogate, A.M. Wilhelm, A.B. Pandit, Some aspects of the design of sonochemical reactors, Ultrason. Sonochem. (2003), https://doi.org/10.1016/S1350-4177(03)00103-2.

[18] R.J. Wood, J. Lee, M.J. Bussemaker, A parametric review of sonochemistry: Control and augmentation of sonochemical activity in aqueous solutions, Ultrason. Sonochem. 38 (2017) 351–370, https://doi.org/10.1016/j.ultsonch.2017.03.030.

[19] I. Tzanakis, G.S.B. Lebon, D.G. Eskin, K.A. Pericleous, Characterizing the cavitation development and acoustic spectrum in various liquids, Ultrason. Sonochem. 34 (2017) 651–662, https://doi.org/10.1016/j.ultsonch.2016.06.034.

[20] H. Nazari-Mahroo, K. Pasandideh, H.A. Navid, R. Sadighi-Bonabi, How important is the liquid bulk viscosity effect on the dynamics of a single cavitation bubble? Ultrason. Sonochem. 49 (2018) 47–52, https://doi.org/10.1016/j.ultsonch.2018.07.013.

[21] S. El Kantar, H.N. Rajha, N. Boussetta, E. Vorobiev, R.G. Maroun, N. Louka, Green extraction of polyphenols from grapefruit peels using high voltage electrical discharges, deep eutectic solvents and aqueous glycerol, Food Chem. 295 (2019) 165–171, https://doi.org/10.1016/j.foodchem.2019.05.111.

[22] H.K. Ravi, C. Breil, M.A. Vian, F. Chemat, P.R. Venskutonis, Biorefining of bilberry (Vaccinium myrtillus L.) pomace using microwave hydrodiffusion and gravity, ultrasound-assisted, and bead-milling extraction, ACS Sustain Chem. Eng. (2018), https://doi.org/10.1021/acssuschemeng.7b04592.

[23] F.S. Mjalli, N.M.A. Jabbar, Acoustic investigation of choline chloride based ionic liquids analogs, Fluid Phase Equilib. 381 (2014) 71–76, https://doi.org/10.1016/j.fluid.2014.08.017.

[24] P. Wang, C. Cheng, Y. Ma, M. Jia, Degradation behavior of polyphenols in model aqueous extraction system based on mechanical and sonochemical effects induced by ultrasound, Sep. Purif. Technol. 247 (2020) 116967, https://doi.org/10.1016/j.seppur.2020.116967.

[25] A.P.D.F. Machado, B.R. Sumere, C. Mekaru, J. Martinez, R.M.N. Bezerra, M. A. Rostagno, Extraction of polyphenols and antioxidants from pomegranate peel using ultrasound: influence of temperature, frequency and operation mode, Int. J. Food Sci. Technol. (2019) 1–10, https://doi.org/10.1111/ijfs.14194.

[26] Y. Tao, Z. Zhang, D.W. Sun, Kinetic modeling of ultrasound-assisted extraction of phenolic compounds from grape marc: influence of acoustic energy density and temperature, Ultrason. Sonochem. 21 (2014) 1461–1469, https://doi.org/10.1016/j.ultsonch.2014.01.029.

[27] Hansen solubility parameters: a user's handbook, Choice Rev. Online. 37 (2000) 37-3905-37–3905. doi:10.5860/CHOICE.37-3905.

[28] S. Jenkins, Hansen solubility parameters (HSP), 2011.

[29] T. Correlation, W. Chemical, T. Numerical, Properties of Polymers (2000), https://doi.org/10.1016/0160-9327(92)90023-I.

[30] S. Hilgenfeldt, M.P. Brenner, S. Grossmann, D. Lohse, Analysis of Rayleigh-Plesset dynamics for sonoluminescing bubbles, J. Fluid Mech. (1998), https://doi.org/10.1017/S0022112098001207.

[31] Y. Son, Simple design strategy for bath-type high-frequency sonoreactors, Chem. Eng. J. 328 (2017) 654–664, https://doi.org/10.1016/j.cej.2017.07.012.

[32] L. Van Wijngaarden, Mechanics of collapsing cavitation bubbles, Ultrason. Sonochem. 29 (2016) 524–527, https://doi.org/10.1016/j.ultsonch.2015.04.006.

[33] L. Milne, I. Stewart, D.H. Bremner, Comparison of hydroxyl radical formation in aqueous solutions at different ultrasound frequencies and powers using the salicylic acid dosimeter, Ultrason. Sonochem. 20 (2013) 984–989, https://doi.org/10.1016/j.ultsonch.2012.10.020.

[34] T.J. Mason, Some neglected or rejected paths in sonochemistry - a very personal view, Ultrason. Sonochem. 25 (2015) 89–93, https://doi.org/10.1016/j.ultsonch.2014.11.014.

[35] B. Khadhraoui, M. Turk, A.S. Fabiano-Tixier, E. Petitcolas, P. Robinet, R. Imbert, M. El Maâtaoui, F. Chemat, Histo-cytochemistry and scanning electron microscopy for studying spatial and temporal extraction of metabolites induced by ultrasound. Towards chain detexturation mechanism, Ultrason. Sonochem. 42 (2018) 482–492, https://doi.org/10.1016/j.ultsonch.2017.11.029.

[36] D. Pingret, A.-S. Fabiano-Tixier, C. Le Bourvellec, C.M.G.C. Renard, F. Chemat, Lab and pilot-scale ultrasound-assisted water extraction of polyphenols from apple pomace, J. Food Eng. 111 (2012) 73–81, https://doi.org/10.1016/j.jfoodeng.2012.01.026.

[37] F. Chemat, N. Rombaut, A.G. Sicaire, A. Meullemiestre, A.S. Fabiano-Tixier, M. Abert-Vian, Ultrasound assisted extraction of food and natural products. Mechanisms, techniques, combinations, protocols and applications. A review, Ultrason. Sonochem. 34 (2017) 540–560, https://doi.org/10.1016/j.ultsonch.2016.06.035.

[38] A. del P. Sánchez-Camargo, M. Bueno, F. Parada-Alfonso, A. Cifuentes, E. Ibáñez, Hansen solubility parameters for selection of green extraction solvents, TrAC - Trends Anal. Chem. 118 (2019) 227–237. doi:10.1016/j.trac.2019.05.046.

[39] J.P. Teas, Graphic analysis of resin solubilities, J. Paint Technol. (1968).

[40] E.J. Llorent-Martínez, G. Zengin, K.I. Sinan, R. Polat, D. Canlı, M.C.N. Picot-Allain, M.F. Mahomoodally, Impact of different extraction solvents and techniques on the biological activities of Cirsium yildizianum (Asteraceae: Cynareae), Ind. Crops Prod. (2020), https://doi.org/10.1016/j.indcrop.2019.112033.

[41] T. Brás, L.A. Neves, J.G. Crespo, M.F. Duarte, Effect of extraction methodologies and solvent selection upon cynaropicrin extraction from Cynara cardunculus leaves, Sep. Purif. Technol. 236 (2020) 116283, https://doi.org/10.1016/j.seppur.2019.116283.

[42] M.G. Contreras-Hernández, L.A. Ochoa-Martínez, J.G. Rutiaga-Quiñones, N.E. Rocha-Guzmán, T.E. Lara-Ceniceros, J.C. Contreras-Esquivel, L.A. Prado Barragán, O.M. Rutiaga-Quiñones, Effect of ultrasound pre-treatment on the physicochemical composition of Agave durangensis leaves and potential enzyme production, Bioresour. Technol. 249 (2018) 439–446. doi:https://doi.org/10.1016/j.biortech.2017.10.009.

[43] A.V. Karim, A. Shriwastav, Degradation of ciprofloxacin using photo, sono, and sonophotocatalytic oxidation with visible light and low-frequency ultrasound: degradation kinetics and pathways, Chem. Eng. J. (2020), https://doi.org/10.1016/j.cej.2020.124853.

[44] M. Ashokkumar, D. Sunartio, S. Kentish, R. Mawson, L. Simons, K. Vilkhu, C. (Kees) Versteeg, Modification of food ingredients by ultrasound to improve functionality: a preliminary study on a model system, Innov. Food Sci. Emerg. Technol. 9 (2008) 155–160. doi:10.1016/j.ifset.2007.05.005.

[45] M. Ashokkumar, L.A. Crum, C.A. Frensley, F. Grieser, T.J. Matula, W.B. McNamara, K.S. Suslick, Effect of solutes on single-bubble sonoluminescence in water, J. Phys. Chem. A. (2000), https://doi.org/10.1021/jp000463r.

[46] J. Lee, M. Ashokkumar, S. Kentish, F. Grieser, Effect of Alcohols on the Initial Growth of Multibubble Sonoluminescence, (2006) 17282–17285. doi:10.1021/jp063320z.

[47] M. Ashokkumar, P. Mulvaney, F. Grieser, The effect of pH on multibubble sonoluminescence from aqueous solutions containing simple organic weak acids and bases, J. Am. Chem. Soc. 121 (1999) 7355–7359, https://doi.org/10.1021/ja990482i.

[48] J. Guan, T.J. Matula, Time Scales for Quenching Single-Bubble Sonoluminescence in the Presence of Alcohols, (2003) 8917–8921. doi:10.1021/jp026494z.

[49] M. Matsuoka, J. Jin, Sonochemiluminescence from lucigenin in an aqueous solution using alcohols as coreactant, Chem. Lett. 44 (2015) 1759–1761, https://doi.org/10.1246/cl.150838.

[50] M. Ashokkumar, J. Lee, Y. Iida, K. Yasui, T. Kozuka, T. Tuziuti, A. Towata, Spatial distribution of acoustic cavitation bubbles at different ultrasound frequencies, ChemPhysChem 11 (2010) 1680–1684, https://doi.org/10.1002/cphc.200901037.

[51] I.A. Saleh, M. Vinatoru, T.J. Mason, N.S. Abdel-Azim, E.A. Aboutabl, F. M. Hammouda, A possible general mechanism for ultrasound-assisted extraction (UAE) suggested from the results of UAE of chlorogenic acid from Cynara scolymus L. (artichoke) leaves, Ultrason. Sonochem. 31 (2016) 330–336, https://doi.org/10.1016/j.ultsonch.2016.01.002.

[52] T. Inoue, A. Yoshinaga, K. Takabe, T. Yoshioka, K. Ogawa, M. Sakamoto, J. I. Azuma, Y. Honda, In situ detection and identification of hesperidin crystals in satsuma mandarin (Citrus unshiu) peel cells, Phytochem. Anal. 26 (2015) 105–110, https://doi.org/10.1002/pca.2541.

[53] A. Smeriglio, L. Cornara, M. Denaro, D. Barreca, B. Burlando, J. Xiao, D. Trombetta, Antioxidant and cytoprotective activities of an ancient Mediterranean citrus (Citrus lumia Risso) albedo extract: microscopic observations and polyphenol characterization, Food Chem. 279 (2019) 347–355, https://doi.org/10.1016/j.foodchem.2018.11.138.

[54] J. Chen, J. Yang, L. Ma, J. Li, N. Shahzad, C.K. Kim, Author Correction: Structure-antioxidant activity relationship of methoxy, phenolic hydroxyl, and carboxylic acid groups of phenolic acids (Scientific Reports, (2020), 10, 1, (2611), 10.1038/s41598-020-59451-z), Sci. Rep. 10 (2020) 1–9. doi:10.1038/s41598-020-62493-y.